2018 IEEE Intelligent Vehicles Symposium (IV)
Changshu, Suzhou, China, June 26-30, 2018

Online Adaptive Covariance Estimation Approach for Multiple Odometry Sensors Fusion

Mostafa Osman[1*], Ahmed Hussein[2], Abdulla Al-Kaff[2], Fernando García[2] and José María Armingol[2]

***Abstract*— Odometry is a crucial task in the design of intelligent vehicles and there are many novel approaches with different sensors in Intelligent Transportation Systems (ITS) field. Accordingly, this leads to the use of multiple methods and sensors for identifying the vehicle pose in the environment, hence the necessity of multiple odometry sensors fusion methods. Quantifying the uncertainties of the sensors used in the vehicle is essential for utilizing effective fusion systems. Since the identification of the true values of the uncertainties is an exhaustive task, this paper introduces an online adaptive covariance estimation approach for drift suffering proprioceptive sensors, using an exteroceptive sensor with known uncertainty. To validate the proposed approach, three scenarios were selected and various experiments were carried out under different conditions. Though the use of multiple odometry sensors fusion algorithm, a comparative study was conducted between the adaptive covariance and several constant covariances based on the true variances. The obtained results show high performance of the proposed approach, in terms of four evaluation metrics for both translation and orientation mean errors.**

I. Introduction

The last global status report on road safety indicates that over 1.2 million fatalities, and up to 50 million injuries annually caused traffic accidents [1]. The majority of these accidents are caused by human error. Accordingly, intelligent vehicles have encountered a significant focus in the Intelligent Transportation Systems Society (ITSS); in order to reduce accidents and traffic congestion.

The localization system is considered as one of the important parts in any intelligent vehicle. The accuracy of the localization system must be as high as possible; in order to avoid any catastrophic maneuver. Sensors of high accuracy data are available for many decades; however, they are still unaffordable for mass production. Therefore, it is required to increase the accuracy of the localization using multiple cost-efficient sensors, which is achieved by the calibration, modeling, filtering and fusion processes. The good knowledge about the covariances and the identification of the uncertainties are fundamental; in order to obtain a filter close to optimal. Tuned and constant covariance parameters are widely used in different works [2], [3]; this is due to the simplicity of the calculations. However, it is not sufficient because the uncertainty in the drift suffering sensors changes with operating conditions, which leads to sub-optimal fusion results. Moreover, it needs a significant number of trails to obtain tolerable results.

Several methods have been presented to estimate the noise covariance matrices; such as correlation techniques that are based on Autocovariance Least-Square method (ALS) [4], [5], Covariance Matching (CM) [6], [7], maximum likelihood [8], [9], and Bayesian estimation [10], [11]. These previous methods usually estimates the covariances of linear systems, except CM methods which deal with nonlinear systems, however it is a non-optimal estimator.

Other works used Adaptive Kalman filters; in order to estimate the covariance matrices [12]. In [13], a Kalman filter with recursive estimation has been presented; to estimate the noise covariance matrix from the measurement sequence of linear time-invariant systems. Additionally, in [14], a stability analysis has been performed to verify the state of the estimator. However, the obtained results were based on simulations, furthermore, the estimation algorithm is efficient with linear systems.

Using filters requires accurate covariances for all the sensors being fused, however, determining the exact values of these covariances is difficult, due to the absence of a ground truth for the exact estimation. Moreover, the values of these covariances might change during the operation of the vehicle. Based on the literature, it is common to manual tune these covaraince, which lead to the filters to operate sub-optimally and obtain worse results.

Accordingly, this paper proposes an online adaptive estimation for the of the noise covariance matrix Q for drift suffering proprioceptive sensors, using an exteroceptive sensor with known uncertainty. This estimation is independent of the factors that affect the sensor reading, and it is not subjected to the accumulation of the error, but to the random white noise error. A comparative study was conducted using multiple odometry sensors fusion algorithm for validation of the approach efficiency and functionality.

The remainder of this paper is organized as follows; section II introduces the formulation of proprioceptive sensors error, followed by the description of the proposed covariance estimation algorithm in section III. Section IV discusses the setup for the experiments, the scenarios used and the evaluation metrics.In Section V the experimental results are discussed. Finally, in section VI conclusions are summarized.

II. Problem Formulation

In this section, the problem formulation of the proprioceptive sensor error model is introduced, moreover, the vehicle kinematics modeling is presented.

[1]Autotronics Research Lab (ARL), Ain Shams University (ASU), Cairo, Egypt mostafaosman144@gmail.com

[2]Intelligent Systems Lab (LSI) Research Group, Universidad Carlos III de Madrid (UC3M), Leganés, Madrid, Spain {ahussein, akaff, fegarcia, armingol}@ing.uc3m.es

*Corresponding Author

A. Proprioceptive Sensors Error Model

On the one hand, proprioceptive sensors measure internal states of the vehicle. For example, wheel optical encoders measure the position of the wheels, accelerometers measure the vehicle accelerations, and digital compasses or gyroscopes measure the vehicle heading angle. On the other hand, exteroceptive sensors acquire information from external observations; such as GPS modules [15].

Moreover, proprioceptive sensors suffer from the accumulation of error in the vehicle pose estimation, which is called the drift error. It is divided into two components: deterministic and stochastic components. The deterministic component includes unequal wheel diameters, misalignment of wheels, or kinematic modeling error due to the inaccuracy of parameters measurement. However, the stochastic component occurs due to the ground condition (slippage), the temperature change, and the driving behavior [16]. Taking both components into consideration, the sensor error is modeled using Equation (1).

$$q^m = (1+\mu)q^t + \varepsilon \tag{1}$$

where q^m and q^t are true and measured variable, μ is the distance dependent scale factor, which models the measured variable dependent errors and ε models the random errors.

The deterministic component can be calibrated [17], however, the stochastic component of the error cannot be eliminated and is variant with different driving conditions. Accordingly, μq and ε are considered random variables, and it is safe to assume that these variables have zero mean Gaussian distribution $\mathcal{N}$, as shown in Equation (2) and (3).

$$\mu q^t \sim \mathcal{N}(0, \sigma_\mu^2) \tag{2}$$

$$\varepsilon \sim \mathcal{N}(0, \sigma_\varepsilon)) \tag{3}$$

Assuming zero mean errors, in case of wheel encoders the value μq^t will be μd^t and is correlated to the Standard Deviation (SD) σ_μ with the correlation constant c, as in (4) and shown in Figure 1.

$$\sigma_{mu} = c\mu q^t \tag{4}$$

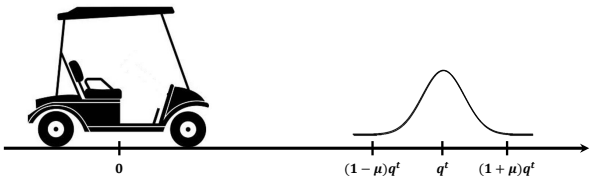

Fig. 1. Distance dependent error in encoder measurements

Accordingly, the proprioceptive error model is:

$$q^m = q^t + \psi \tag{5}$$

$$\psi = \mu q^t + \varepsilon \tag{6}$$

$$\psi \sim \mathcal{N}(0, (c\mu q^t)^2 + \sigma_\varepsilon^2) \tag{7}$$

where σ_ε is the SD of the stochastic component of the error.

B. Kinematic Modeling

The pose of a vehicle is estimated using proprioceptive sensors based on a recursive kinematic model, which calculates the vehicle pose $\mathbf{x}_k$ using the previous pose $\mathbf{x}_{k-1}$ and the input measurement $\mathbf{u}_k$, as shown in Equation (8).

$$\mathbf{x}_k = \mathbf{f}(\mathbf{x}_{k-1}, \mathbf{u}_k) \tag{8}$$

where $\mathbf{u}_k$ is the distance traveled and steering angle in case of encoders, yaw angle in case of a digital compass or a gyroscope, and accelerations in case of an accelerometer.

The pose of the vehicle is computed recursively, using the previous pose $\mathbf{x}_{k-1}$ and the input to the vehicle $\mathbf{u}_k$, as illustrated in Equations (9), (10) and (11).

$$\begin{aligned}\hat{\mathbf{x}}_\mathbf{k} &= \mathbf{f}(\hat{\mathbf{x}}_{k-1}, \mathbf{u}_k) \\ &= \begin{bmatrix} x_{k-1} \\ y_{k-1} \\ \theta_{k-1} \end{bmatrix} + \begin{bmatrix} \Delta d_k^e cos(\theta_{k-1} + \Delta\theta_k^e/2) \\ \Delta d_k^e sin(\theta_{k-1} + \Delta\theta_k^e/2) \\ \theta_{k-1} + \Delta\theta_k^e \end{bmatrix}\end{aligned} \tag{9}$$

$$\mathbf{u}_k = \begin{bmatrix} \Delta d_k^e \\ \Delta\theta_k^e \end{bmatrix} \tag{10}$$

$$\Delta\theta = \frac{\Delta d_k^e}{L} tan(\varphi^s) \tag{11}$$

where Δd_k^m is the incremental distance covered in the last iteration, φ_k^s is the instantaneous steering angle of the vehicle, and L is the vehicle wheelbase.

III. Covariance Estimation

Given the kinematic model of the vehicle, and using Equation (5) for quantifying the error in a proprioceptive sensor, the generalized error model and the covariance for the inputs are presented in Equations (12) and (13) respectively.

$$\mathbf{u} = \begin{bmatrix} q_1^m \\ \vdots \\ q_n^m \end{bmatrix} = \begin{bmatrix} q_1^t + \psi^e \\ \vdots \\ q_n^t + \psi^s \end{bmatrix} \tag{12}$$

$$Q_u = \begin{bmatrix} (c_0\mu_0 q_0^t)^2 + \sigma_0^2 & \dots & 0 \\ \vdots & \ddots & \vdots \\ 0 & \dots & (c_n\mu_n q_n^t)^2 + \sigma_n^2 \end{bmatrix} \tag{13}$$

The exteroceptive sensor measurement in the world frame $\mathcal{N}(\mathbf{Z}, \mathbf{R})$ is shown in Equation (14).

$$\mathbf{Z_k} = \begin{bmatrix} x_k^o \\ y_k^o \\ \theta_k^o \end{bmatrix} \text{ and } \mathbf{R} = \begin{bmatrix} \sigma_{xx} & \sigma_{xy} & \sigma_{x\theta} \\ \sigma_{yx} & \sigma_{yy} & \sigma_{y\theta} \\ \sigma_{\theta x} & \sigma_{\theta y} & \sigma_{\theta\theta} \end{bmatrix} \tag{14}$$

where x_k^o, y_k^o and θ_k^o are the observed vehicle states.

The true pose $\mathbf{x}$ most likely lies in the confidence ellipse of the measurement defined by the Eigenvalues of $\mathbf{R}$, as shown in the Figure 2. Hence, using the square root of

the covariance matrix, a set of points in the observation distribution (sigma points) at time instance k is computed according to [18] and shown in Equation (15).

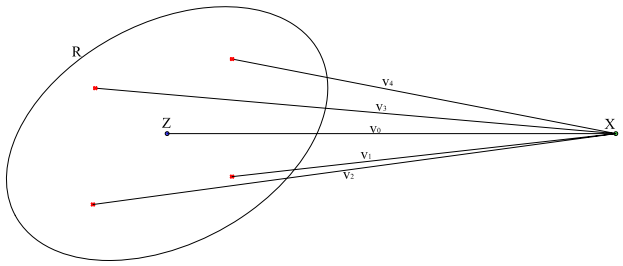

Fig. 2. Calculating the sigma points innovation for covariance estimation

$$\xi_k = \begin{bmatrix} \mathbf{Z}_k & \mathbf{Z}_k + (\alpha\sqrt{\mathbf{R}_k}) & \mathbf{Z}_k - (\alpha\sqrt{\mathbf{R}_k}) \end{bmatrix} \tag{15}$$

where α is a scaling constant which depends on the accuracy of the used sensor, along with the accuracy of exteroceptive sensor covariance matrix.

In order to ensure vehicle pose lies inside the confidence ellipse of the exteroceptive sensor, a method for neglecting the outliers is implemented; using Mahalanobis distance thresholding as shown in Equation (16) and (17), where the estimated pose is used instead of the true pose, since the vehicle actual pose is unknown.

$$\hat{\mathbf{v}}_k^T \mathbf{R} \hat{\mathbf{v}}_k < g^2 \tag{16}$$

$$v_k = \hat{\mathbf{x}}_\mathbf{k} - \mathbf{Z}_\mathbf{k} \tag{17}$$

where g^2 is the Mahalabonis threshold and v_k is the innovation between exeroceptive and propriocetpive observations.

Using the sigma points, the sigma innovation points are sampled with Equation (18), and the innovation is mapped to the sensor space with Equation (19).

$$\mathbf{v}_\zeta = \begin{bmatrix} \mathbf{v}_{\zeta_0} & \mathbf{v}_{\zeta_1} & \dots & \mathbf{v}_{\zeta_6} \end{bmatrix} \text{ where } \mathbf{v}_{\zeta_i} = \xi_k^i - \hat{\mathbf{x}}_k \tag{18}$$

$$\mathbf{v}_{\zeta_i}^m = \mathbf{M}(\mathbf{v}_{\zeta_i}) \tag{19}$$

where $\mathbf{M}$ is a mapping function from the world frame $\mathbf{v}_{\zeta_i}$ to the sensor space $\mathbf{v}_{\zeta_i}^m$.

For example, in case of encoders, the function $\mathbf{M}$ is represented in Equation (20).

$$\begin{bmatrix} v_{\zeta_i}^e \\ v_{\zeta_i}^s \end{bmatrix} = \begin{bmatrix} \| v_{x_i} + v_{y_i} \|_2 \\ v_{\theta_i} \end{bmatrix} \tag{20}$$

After computing the innovation in the sensor space, the value is concatenated in a matrix that is referred as innovation memory matrix Ξ as shown in Equation (21), where the choice of the size of the innovation memory matrix n should be a trade-off between accuracy in estimation and the computational cost.

$$\Xi^{q_j} = \begin{bmatrix} \mathbf{v}_{\zeta_{k-n}}^e \\ \mathbf{v}_{\zeta_{k-n+1}}^e \\ \vdots \\ \mathbf{v}_{\zeta_k}^e \end{bmatrix} \tag{21}$$

An exteroceptive sensor does not suffer from error accumulation, but only from random error, therefore using the innovation memory matrix Ξ, the measured variable dependent scale factor μ is estimated by computing the first order polynomial fit of the innovation data, using linear least squares approach, as shown in Equation (22).

$$\begin{bmatrix} \mu_0 \\ \hat{\mu}_{1_i}^{q_j} \end{bmatrix} = (\mathbf{K}^T \cdot \mathbf{K}) \mathbf{K}^T \mathbf{\Xi}_i^{q_j} \tag{22}$$

where $\mathbf{K}$ is the time vector for the last n instances, $\Xi_i^{q_j}$ is the i^{th} column of the innovation memory matrix of the j^{th} measured quantity, and $\hat{\mu}_{1_i}^{q_j}$ is the estimated scale factor computed from the i^{th} sigma innovation for the j^{th} measured variable q_j, as shown in Equation (23).

$$\hat{\mu}_1^{q_j} = \begin{bmatrix} \hat{\mu}_{1_0}^{q_j} & \dots & \hat{\mu}_{1_6}^{q_j} \end{bmatrix} \tag{23}$$

Accordingly, the measured variable dependent scale factor μ is estimated by calculating the weighted mean of $\hat{\mu}_1^{q_j}$, as shown in Equation (24).

$$\hat{\mu}^{q_j} = \sum_{i=0}^{6} W_i^{(m)} \hat{\mu}_{1_i}^{q_j} \tag{24}$$

In this paper, the weights are adjusted as shown in Equation (25), however, they can be modified according to the user preference, where $W_i^{(m)}$ is weight of the i^{th} scale factor.

$$W_0^{(m)} = \frac{L}{2L+1} \text{ and } W_0^{(m)} = \frac{L+1}{4L^2+2L} \tag{25}$$

Therefore, using $\hat{\mu}^{q_j}$, the propriocetpive sensor covariance matrix is approximated as shown in Equation (26).

$$Q_u \approx \begin{bmatrix} (c_0 \hat{\mu}^0 q_0^m)^2 + \varepsilon_0^2 & \dots & 0 \\ \vdots & \ddots & \vdots \\ 0 & \dots & (c_n \hat{\mu}^n q_n^m)^2 + \varepsilon_n^2 \end{bmatrix} \tag{26}$$

where ε is a parameter representing the stochastic component of the propriocetpive sensor error, and c is adjusted according to the sensor performance.

IV. Experimental Work

In order to validate the proposed approach, several scenarios are designed and tested over various experiments. This section describes the used platform for the real-word experiments, the testing environment, the designed scenarios, and the selected evaluation metrics.

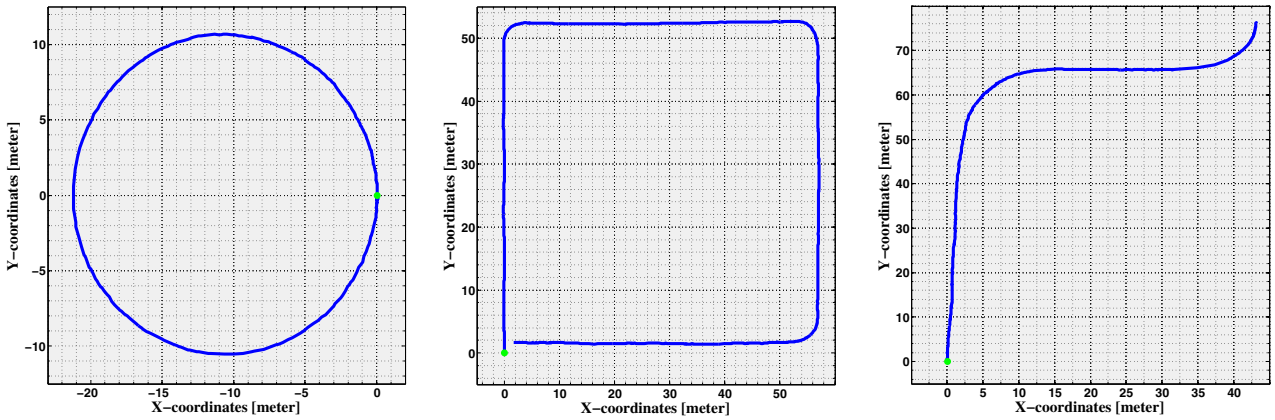

Scenario I Scenario II Scenario III

Fig. 3. Visual demonstration of the three scenarios, where the green point is the start point and the blue curve is the path drawn using the lidar odometry

A. Setup

The aforementioned approach was tested over an automated ground vehicle, which is a part of the Intelligent Campus Automobile (iCab) project [19]. The vehicle is an electric golf cart, which is equipped with multiple on-board sensors, including lidar, stereo camera, optical encoders for wheel and steering, digital magnetometer and GPS module. Moreover, the vehicle is equipped with an embedded computer, which operates with Robot Operating System (ROS) based architecture [20]. This architecture enables the vehicles to perform self localization, navigation, planning and environment perception, among others.

B. Scenarios

The testing environment was the off-road vicinity of the campus, which has free pedestrian areas and surrounded with many buildings. In this environment, three scenarios were designed to evaluate the proposed approach, and each scenario was experimented three times under different conditions. The scenarios are depicted in Figure 3 and described in the following sub-sections.

1) Scenario I: The first scenario was designed as a circle of total diameter of $22m$, in which the iCab steering wheel was adjusted to 8.5^o and average velocity of $5kmph$. In this case, the theoretical path was designed as a pure circle with the same diameter to be compared with the obtained odometries. The scenario was selected to evaluate the proposed approach performance in optimizing the localization in simple circular motion. Moreover, it is a closed-loop, thus the vehicle end point is the same as the starting point.

2) Scenario II: The second scenario was designed as a quadratic shape of total length of $54m$ and width of $56m$. This was also a closed shape, where the theoretical path was designed as a right-angled quadratic shape, thus the vehicle end point is the same as the starting point. The iCab followed the shape with average velocity of $5kmph$ and rotating with sharp 30^o around the corners. The scenario was selected to evaluate the proposed approach performance in optimizing the localization in both straight-line and curved motions.

3) Scenario III: The third and last scenario was designed as a trajectory from one building to another in the campus. The selected points are part of the pick-up / drop-off points of the iCab project. The theoretical path was obtained from the path planner to be compared with the obtained odometries. The path consists of multiple curves, straight-lines, dynamic obstacles, and it is one of the normal trajectories that the iCab follows in its daily operation. The iCab followed the path with average velocity of $5kmph$ and a maximum of 15^o steering angle during curvatures.

C. Evaluation Metrics

In order to evaluate the true potential of the proposed algorithm, the performance and results are compared relative to different values of constant covariances in a fusion algorithm, and the `robot_localization` package was selected for the fusion [21]. The package contains two fusion algorithms: Extended Kalman Filter (EKF) and Unscented Kalman Filter (UKF). In this paper, the UKF was used for the nonlinearity aspect of the vehicle model. The decision to use this package was to eliminate the factors of errors in the fusion algorithm implementation, thus focusing on the effect of using different covariances under the same conditions.

The evaluation metrics for the Ackermann model are calculated for both, translation and orientation. Firstly, the mean and maximum error percentages of the translation; which are calculated as shown in Equations (27) and (28) respectively.

$$TE_{mean}[\%] = \frac{\frac{1}{N}\sum_{k=1}^{N}\left\|\begin{bmatrix}\hat{x}_k\\ \hat{y}_k\end{bmatrix} - \begin{bmatrix}x_k\\ y_k\end{bmatrix}\right\|_2}{TotalDistance} \tag{27}$$

$$TE_{max}[\%] = \frac{\frac{1}{N}max(\left\|\begin{bmatrix}\hat{x}_k\\ \hat{y}_k\end{bmatrix} - \begin{bmatrix}x_k\\ y_k\end{bmatrix}\right\|_2)}{TotalDistance} \tag{28}$$

where $(\hat{x}_k, \hat{y}_k)$ are the estimated coordinates of the vehicle and (x_k, y_k) are the true coordinates at time step k.

As for the orientation, the mean and maximum error in the orientation are divided by the total distance covered by

the vehicle, which are calculated as shown in Equations (29) and (30) respectively.

$$OE_{mean}[^o/m] = \frac{\frac{1}{N}\sum_{k=1}^{N} \hat{\theta}_k - \theta_k}{TotalDistance} \tag{29}$$

$$OE_{max}[^o/m] = \frac{\frac{1}{N} max(\hat{\theta}_k - \theta_k)}{TotalDistance} \tag{30}$$

where $\hat{\theta}_k$ is the estimated orientation of the vehicle and θ_k is the true orientation of the vehicle at time step k.

The reason for selecting these metrics is due to the fact that iCab utilizes Lidar Odometry and Mapping (LOAM) package [22]. Since the package accuracy over the KITTI Benchmark is in the second place in the list of the most efficient odometry algorithms, with values of 0.64% and $0.0014^o/m$ for the TE_{mean} and OE_{mean} respectively. Therefore, LOAM readings were considered as the closest to ground-truth in comparison with all other available sensors in the iCab, and accordingly it was set as the reference odometry for comparisons in the metrics estimation.

V. Results and Discussion

In the experiments, five different odometries were executed in the iCab platform; the lidar as the reference odometry, GPS as the exteroceptive sensor odometry and wheel encoders as the propriocetpive sensor odometry. Additionally, visual odometry and compass orientation were included as more inputs to the fusion algorithm. The covariance estimation was estimated for the propriocetpive sensor based on the available covariance of the exteroceptive sensor.

In order to show the efficacy of the covariance estimation algorithm, the results are compared to the results using different values of constant covariances. The values used are percentages of the True Variances (T.V.) of both the steering encoder and the translation encoder, which are calculated retroactively from the data of the experiments.

The parameters values used for the covariance estimation algorithm is the same in all scenarios, in order to ensure that the algorithm does not need different parameters for different scenarios and to insure the applicability and practicality of it. During all experiments, the exteroceptive sensor parameters were as follows: α was set to 0.5, c_e and c_s were set to 0.05, and ε_e and ε_s were set to 0.

Finally, the constant values of covariances are selected depending on the error values for each experiment. As shown in the tables below, 125% of the T.V. gave higher error than 25% of the T.V.. Observing these results, smaller percentages of the T.V. were used in order to reach better results. And lower than 2.5% of the T.V. were omitted, because they gave larger errors.

A. Scenario I

Table I shows the experimental quantitative results of the first scenario, comparing the proposed approach of covariance estimation against the T.V. at four different values. The obtained results show the covariance estimation algorithm outperforming all T.V. values in both translation error and orientation error. All performed trials of T.V. obtained near results at different values. There might be a chance that with more trials of different values of T.V., one of them could outperform the proposed approach, however, the tuning issue consumes time and efforts.

TABLE I
MEAN OF THE 3 SCENARIO I EXPERIMENTS RESULTS

Metrics	Mean [%]		Mean [$^o/m$]	
	TE_{mean}	TE_{max}	OE_{mean}	OE_{max}
Adaptive	1.743	3.043	0.0029	0.097
True Variance	6.756	13.853	0.249	0.612
2.5% T.V.	1.796	3.598	0.077	0.227
5% T.V.	2.619	5.705	0.099	0.302
25% T.V.	4.061	7.746	0.164	0.349
125% T.V.	7.613	14.772	0.263	0.667

B. Scenario II

Table II shows the experimental quantitative results of the second scenario, comparing the proposed approach of covariance estimation against the T.V. at four different values. The obtained results show that the proposed approach was able to outperform the T.V. in the translation errors. However, it obtained minimal error of 0.0001^o in the mean orientation in comparison to one of the T.V., despite having the best maximum orientation error.

TABLE II
MEAN OF THE 3 SCENARIO II EXPERIMENTS RESULTS

Metrics	Mean [%]		Mean [$^o/m$]	
	TE_{mean}	TE_{max}	OE_{mean}	OE_{max}
Adaptive	3.047	4.717	0.020	0.089
True Variance	13.034	44.662	0.019	0.109
2.5% T.V.	4.942	8.259	0.019	0.111
5% T.V.	6.498	11.451	0.019	0.103
25% T.V.	9.633	21.433	0.020	0.111
125% T.V.	13.593	60.060	0.019	0.110

C. Scenario III

Table III shows the experimental quantitative results of the second scenario, comparing the proposed approach of covariance estimation against the T.V. at four different values. The obtained results show that the proposed approach was able to outperform the T.V. maximum errors in both translation and orientation. However, for the mean errors, it obtained a minimal error value of 0.098% in the mean translation error, and a minimal error value of 0.003^o in the mean orientation error. This is taking into consideration that the best mean translation error was obtained at 2.5% of the T.V., while the best mean orientation error was obtained at the exact value of the T.V., which implies that the proposed approach outperforms in general all T.V. values.

TABLE III

MEAN OF THE 3 SCENARIO III EXPERIMENTS RESULTS

Metrics	**Mean** [%]		**Mean** [$^o/m$]	
	TE_{mean}	TE_{max}	OE_{mean}	OE_{max}
Adaptive	4.473	7.545	0.025	0.085
True Variance	15.841	56.230	0.022	0.167
2.5% T.V.	4.375	8.971	0.023	0.090
5% T.V.	4.613	10.372	0.024	0.120
25% T.V.	7.627	21.715	0.025	0.147
125% T.V.	13.508	46.674	0.024	0.155

D. Discussion

The proposed covariance estimation algorithm has consistent results in all proposed scenarios and experiments, which proves its efficacy. This proves that using constant covariances with a sensor that suffers from drift error is neither optimal nor practical, since the variance of the sensor changes drastically from one operation to another. Moreover, it is shown that the error in these sensors, using a constant covariance, changes depending on operating and stochastic conditions.

VI. CONCLUSION

The most widely used approach for localization is multi-sensor fusion using probabilistic filters. This approach fuses the readings from different proprioceptive and exteroceptive sensors to estimate a more precise pose. Fusion requires sensors uncertainties (covariances), however, determining the exact values of these covariances is difficult, due to the absence of a ground truth for the exact estimation.

This paper presents an online covariance estimation algorithm for drift suffering proprioceptive sensors, which uses an exteroceptive sensor with known covariance. The strength of the algorithm is not just the ability to approximate the true covariance, but also the adaptiveness to different operating conditions, unlike the constant covariances, at which the variance of the sensor changes drastically from one operation to another.

Different scenarios were designed to test the algorithm, where each scenario was carried out three times in order to test the efficacy of the algorithm compared to constant covariances of different values. The results showed that the proposed approach outperformed constant covariances, in case of translation errors and orientation errors in the majority of experiments. Despite the fact that the proposed approach did not outperform constant covariances in every single metric of all experiments, the obtained results were always very close to the best one, which differed in value from one experiment to another and at different T.V. instances.

ACKNOWLEDGMENT

This research is supported by Madrid Community project SEGVAUTO-TRIES (S2013-MIT-2713) and by the Spanish Government CICYT projects (TRA2015-63708-R and TRA2016-78886-C3-1-R).

REFERENCES

[1] W. H. Organization, *Global status report on road safety 2015*. World Health Organization, 2015.

[2] G. Cotugno, L. D'Alfonso, W. Lucia, P. Muraca, and P. Pugliese, "Extended and unscented kalman filters for mobile robot localization and environment reconstruction," in *21st Mediterranean Conference on Control & Automation (MED)*. IEEE, 2013, pp. 19–26.

[3] M. A. Skoglund, G. Hendeby, and D. Axehill, "Extended kalman filter modifications based on an optimization view point," in *Information Fusion (Fusion), 2015 18th International Conference on*. IEEE, 2015, pp. 1856–1861.

[4] J. Duník, O. Straka, and M. Šimandl, "On autocovariance least-squares method for noise covariance matrices estimation," *IEEE Transactions on Automatic Control*, vol. 62, no. 2, pp. 967–972, 2017.

[5] M. A. Zagrobelny and J. B. Rawlings, "Practical improvements to autocovariance least-squares," *AIChE Journal*, vol. 61, no. 6, pp. 1840–1855, 2015.

[6] Y. Meng, S. Gao, Y. Zhong, G. Hu, and A. Subic, "Covariance matching based adaptive unscented kalman filter for direct filtering in ins/gnss integration," *Acta Astronautica*, vol. 120, pp. 171–181, 2016.

[7] W. Zhang, W. Shi, and Z. Ma, "Adaptive unscented kalman filter based state of energy and power capability estimation approach for lithium-ion battery," *Journal of Power Sources*, vol. 289, pp. 50–62, 2015.

[8] M. A. Zagrobelny and J. B. Rawlings, "Identifying the uncertainty structure using maximum likelihood estimation," in *American Control Conference (ACC), 2015*. IEEE, 2015, pp. 422–427.

[9] A. Aubry, A. De Maio, L. Pallotta, and A. Farina, "Maximum likelihood estimation of a structured covariance matrix with a condition number constraint," *IEEE Transactions on Signal Processing*, vol. 60, no. 6, pp. 3004–3021, 2012.

[10] Z. Weng and P. M. Djurić, "A bayesian approach to covariance estimation and data fusion," in *Signal Processing Conference (EUSIPCO), 2012 Proceedings of the 20th European*. IEEE, 2012, pp. 2352–2356.

[11] Y. Wang and P. M. Djurić, "Distributed bayesian estimation of linear models with unknown observation covariances," *IEEE Transactions on Signal Processing*, vol. 64, no. 8, pp. 1962–1971, 2016.

[12] S. Akhlaghi, N. Zhou, and Z. Huang, "Adaptive adjustment of noise covariance in kalman filter for dynamic state estimation," *arXiv preprint arXiv:1702.00884*, 2017.

[13] H. Wang, Z. Deng, B. Feng, H. Ma, and Y. Xia, "An adaptive kalman filter estimating process noise covariance," *Neurocomputing*, vol. 223, pp. 12–17, 2017.

[14] B. Feng, M. Fu, H. Ma, Y. Xia, and B. Wang, "Kalman filter with recursive covariance estimation—sequentially estimating process noise covariance," *IEEE Transactions on Industrial Electronics*, vol. 61, no. 11, pp. 6253–6263, 2014.

[15] R. Siegwart, I. R. Nourbakhsh, and D. Scaramuzza, *Introduction to autonomous mobile robots*. MIT press, 2011.

[16] A. Rudolph, "Quantification and estimation of differential odometry errors in mobile robotics with redundant sensor information," *The International Journal of Robotics Research*, vol. 22, no. 2, pp. 117–128, 2003.

[17] K. Lee, W. Chung, and K. Yoo, "Kinematic parameter calibration of a car-like mobile robot to improve odometry accuracy," *Mechatronics*, vol. 20, no. 5, pp. 582–595, 2010.

[18] E. A. Wan and R. Van Der Merwe, "The unscented kalman filter for nonlinear estimation," in *Adaptive Systems for Signal Processing, Communications, and Control Symposium 2000. AS-SPCC. The IEEE 2000*. Ieee, 2000, pp. 153–158.

[19] P. Marin-Plaza, J. Beltran, A. Hussein, B. Musleh, D. Martin, A. de la Escalera, and J. M. Armingol, "Stereo vision-based local occupancy grid map for autonomous navigation in ros," *Joint Conference on Computer Vision, Imaging and Computer Graphics Theory and Applications (VISIGRAPP)*, vol. 3, pp. 703–708, 2016.

[20] A. Hussein, P. Marin-Plaza, D. Martin, A. de la Escalera, and J. M. Armingol, "Autonomous off-road navigation using stereo-vision and laser-rangefinder fusion for outdoor obstacles detection," *IEEE Intelligent Vehicles Symposium (IV)*, pp. 104–109, 2016.

[21] T. Moore and D. Stouch, "A generalized extended kalman filter implementation for the robot operating system," in *Proceedings of the 13th International Conference on Intelligent Autonomous Systems (IAS-13)*. Springer, July 2014.

[22] J. Zhang and S. Singh, "Loam: Lidar odometry and mapping in real-time." in *Robotics: Science and Systems*, vol. 2, 2014.